Available online at www.sciencedirect.com
ScienceDirect
Journal of Power Sources 164 (2007) 415–424
JOURNAL OF POWER SOURCES
www.elsevier.com/locate/jpowsour

Impedance analysis on electric double layer capacitor with transmission line model

Masayuki Itagaki [a,*], Satoshi Suzuki [a], Isao Shitanda [a], Kunihiro Watanabe [a], Hiroshi Nakazawa [b]

[a] *Department of Pure and Applied Chemistry, Faculty of Science and Technology, Tokyo University of Science, Noda, Chiba 278-8510, Japan*
[b] *Honda R&D, Hagamachi, Tochigi 321-3393, Japan*

Received 6 September 2006; received in revised form 26 September 2006; accepted 27 September 2006
Available online 13 November 2006

Abstract

A new electrode model involving the fractal structure of activated carbon used as electrode material was proposed for an electric double layer capacitor (EDLC). The fractal structure of activate carbon was simulated by branch pore structure of three sizes of cylindrical pores. Three sizes of cylindrical pores were related to macro, meso, and micro pore, since the pore size of activated carbon has wide distribution with a few modes of nm order. The impedance spectrum of EDLC describes the locus of blocking electrode in low frequency range, and the curve at an angle of almost 45° to real axis in high frequency range on the Nyquist plane. The low and high frequency ranges of the impedance spectrum were defined as a lumped constant-type and a distributed constant-type, respectively. Computer simulation of electrochemical impedance with the present electrode model was carried out to understand the relation between the impedance and the electrode structure. The contributions of five parameters to impedance spectrum were discussed, i.e., depth of pore, diameter of pore, specific resistance, the interfacial impedance at electrode/solution, and branch number. The specific resistance p influenced on the shape of impedance spectrum in distributed constant-type range significantly. On other hand, the interfacial impedance at electrode/solution interface controlled the shape of the impedance spectrum in lumped constant-type range. In the course of the curve-fitting to impedance spectrum of EDLC, the separated impedance spectra related to macro, meso, and micro pores were obtained, and the roles of these pores on electric capacity were discussed.

Keywords: Electric double layer capacitor; Electrochemical impedance spectroscopy; Transmission line model; Fractal structure

1. Introduction

An electric double layer capacitor (EDLC) is an energy conversion device that stores electric charge in the electric double layer at electrode/electrolyte interface. Activated carbon with high surface area is usually used as the electrode material since the usable charge stored in EDLC mainly depends on the surface area. In addition, the usable charge is also related to the pore size and the pore structure. It was reported that the feature of high capacitance in EDLC depended on the characteristics of pore of nm order (micro pore) [1–5]. If the ion radius of electrolyte is large comparing with the pore radius, the ions cannot penetrate completely into the micro pore and all surface area cannot work to store the charge [1,6–9]. Therefore, it can be considered that the pore structure of activated carbon is one of the important factors for capacitance of EDLC. For example, the roles of macro, meso, and micro pores are different to store the charge.

Electrochemical impedance spectroscopy (EIS) allows the information concerning electrochemical and electric properties of electrode and electrolyte. Several time constants in electrode reactions can be discriminated, and the electrode structure can be analyzed by EIS. Therefore, many researchers have used EIS to analyze structure of porous electrode [9–18]. Some groups adopted transmission line model (TLM) to simulate the frequency response in a pore of EDLC. For example, Qu and Shi [6] carried out the curve-fitting to impedance spectrum of EDLC by the assumptions of cylindrical pore with distributed capacitance and resistance in TLM. They [6] discussed the relationship between time constant of charge/discharge and cell voltage. Song et al. [19,20] simulated impedance spectrum of EDLC

* Corresponding author. Tel.: +81 4 7122 9492; fax: +81 4 7123 9890.
E-mail address: itagaki@rs.noda.tus.ac.jp (M. Itagaki).

0378-7753/$ – see front matter © 2006 Elsevier B.V. All rights reserved.
doi:10.1016/j.jpowsour.2006.09.077

Nomenclature

Parameter list of single pore

A	cross-section area of a pore (cm^2)
C_{dl}^{**}	capacitance per unit area ($F\,cm^{-2}$)
dX	depth per segment (cm), $dX = X/N$
D	diameter of a pore (cm)
m	segment number
N	number of partition (piece) ($n = 1$–N)
R_c^{**}	reaction resistance per unit area ($\Omega\,cm^2$)
R_{sol}	solution resistance (Ω)
R_{solseg}	solution resistance per one segment (Ω), $R_{solseg} = R_{sol}^{*}dX$
R_{sol}^{*}	solution resistance per unit length ($\Omega\,cm^{-1}$), $R_{sol}^{*} = \rho/A$
X	depth of a pore (cm)
Z	impedance of a pore (Ω)
Z_{seg}	impedance per one segment (Ω), $Z_{seg} = Z^{*}/dX$ (b)
Z^{*}	impedance per unit length ($\Omega\,cm$), $Z^{*} = Z^{**}/\pi D$ (a)
Z^{**}	impedance per unit area ($\Omega\,cm^2$)

Greek letters

ρ	specific resistance ($\Omega\,cm$)

Parameter list of a pore with repeated structure

A_m	cross-section area of a pore per segment of segment number m (cm^2)
b	branch number
C_{dl}^{**}	capacitance per unit area ($F\,cm^{-2}$)
dX_m	depth of a pore per one segment of segment number m (cm), $dX_m = X_m/N$
D_m	diameter per one segment of segment number m (cm)
N	segment number ($n = 1$–N)
R_c^{**}	reaction resistance per unit area ($\Omega\,cm^2$)
$R_{sol,m}$	solution resistance of segment number m (Ω)
$R_{sol,m}^{*}$	solution resistance per unit length of segment number m ($\Omega\,cm^{-1}$), $R_{sol,m}^{*} = \rho/A_m$
$R_{solseg,m}$	solution resistance per one segment of segment number m (Ω), $R_{sol,m} = R_{sol,m}^{*}dX_m$
X_m	depth of a pore of segment number m (cm)
Z_m	impedance of segment number m (Ω)
Z_m^{*}	impedance per unit length of segment number m ($\Omega\,cm$), $Z_m^{*} = Z^{**}/D_m$
$Z_{seg,m}$	impedance per one segment of segment number m (Ω), $Z_{seg,m} = Z_m^{*}/dX_m$
Z_{total}	total impedance of pore electrode (Ω)
Z^{**}	impedance per unit area ($\Omega\,cm^2$)

Greek letters

ρ	specific resistance ($\Omega\,cm$)

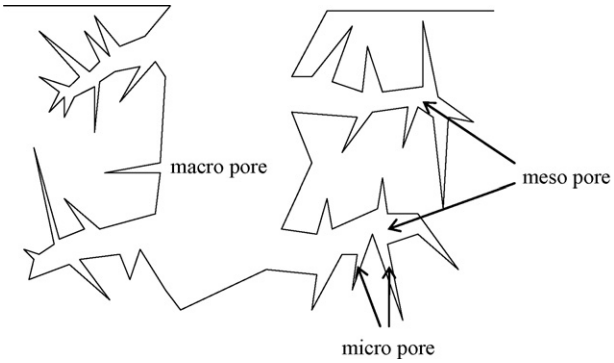

Fig. 1. Conceptual scheme of pore of activated carbon.

by assuming cylindrical pore electrode, and proposed TLM with pore size distribution (TLM-PSD). The simulated results of electrochemical impedance with these models [6,19–20] are in good agreement with experimental ones geometrically. However, the pores of activated carbon have complex branch structure as described in Fig. 1, and it is considered that impedance analysis model should involve the branch pore structure.

In the present paper, we propose a new conceptual model of EDLC with branch pore structure. The single pore electrode is represented by a cylindrical pore. The branch pore structure of activated carbon was simulated by the repetition with three sizes of cylindrical pores in this model. These pores are related to macro, meso, and micro pore in descending order. A great number of branch pores are located on the electrode, and the electrochemical impedance is assessed by sum of the branch pores. Computer simulation of electrochemical impedance with the present electrode model was carried out to characterize the impedance spectrum of EDLC. Furthermore, the contributions of macro, meso, and micro pores to electrochemical impedance of EDLC were studied by the curve fitting to impedance spectrum.

2. Theory

2.1. Lumped constant-type and distributed constant-type equivalent circuits

The schemes of blocking electrochemical impedance that excludes Faradaic process are shown in Fig. 2 for (a) lumped constant-type equivalent circuit and (b) distributed constant-type equivalent circuit. In the present paper, the lumped constant-type equivalent circuit can be expressed as a series of solution

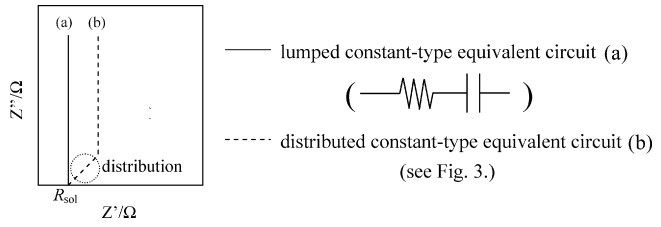

Fig. 2. Schemes of electrochemical impedance of EDLC. (a) Lumped constants equivalent circuit and (b) distributed constants equivalent circuit.

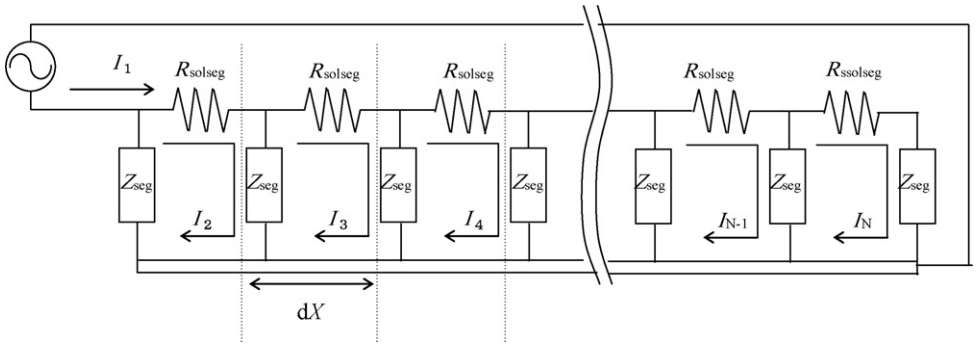

Fig. 3. Distributed constant equivalent circuit of a single pore.

resistance and capacitance. The distributed constant-type equivalent circuit is composed of solution resistance and impedance per one segment as depicted in Fig. 3. The impedance of equivalent circuit (a) describes locus in parallel with the imaginary axis on complex plane. The real part is solution resistance R_{sol}, and the imaginary part converges to zero with high frequency.

The impedance of equivalent circuit (b) has almost similar shape to that of the equivalent circuit (a) in low frequency range. And it describes the locus of 45° to real axis in high frequency range. The reason is that the current distribution on the electrode is non-uniform in high frequency range.

2.2. Theoretical formula of impedance with cylindrical electrode by TLM

Levie [21] solved theoretical formula of TLM impedance for inner wall of cylindrical electrode as follows:

$$Z = \sqrt{R^*_{sol} Z^*}\ \coth \sqrt{\frac{R^*_{sol} X}{Z^*}} \tag{1}$$

$$Z^* = \frac{Z^{**}}{\pi D} \tag{2}$$

$$R^*_{sol} = \frac{\rho}{A} \tag{3}$$

where X is the depth of a pore, D the diameter of a pore, Z^{**} the impedance per unit area, Z^* the impedance per unit length, Z the impedance of a pore, R^*_{sol} the solution resistance per unit length, p the specific resistance, and A is the cross-section area of a pore. Z^{**} including Faradaic process such as redox capacitor is represented by formula (4), and Z^{**} excluding Faradaic process (blocking electrode) is represented by formula (5).

$$Z^{**} = \frac{R^{**}_c}{1 + j\omega R^{**}_c C^{**}_{dl}} \tag{4}$$

$$Z^{**} = \frac{1}{j\omega C^{**}_{dl}} \tag{5}$$

j is the imaginary number unit, ω the angular frequency (=$2\pi f$, f is frequency), R^{**}_c the reaction resistance per unit area, and C^{**}_{dl} is the capacitance per unit area.

2.3. Impedance simulation of single pore by using matrix [22]

In the present paper, impedance spectrum is basically simulated by assuming cylindrical pore as depicted in Fig. 4(a). The cylindrical pore is divided into N segments in the direction of the depth, and each segment is defined as $n = 1, 2, \ldots, N$ from top to bottom of the pore. Impedance per unit area Z^{**} and solution resistance per unit length R^*_{sol} were converted to impedance per one segment Z_{seg} and solution resistance per one segment R_{solseg} by formulas (6)–(8),

$$Z_{seg} = \frac{Z^*}{dX} \tag{6}$$

$$Z^* = \frac{Z^{**}}{\pi D} \tag{7}$$

$$R_{solseg} = R^*_{sol} dX \tag{8}$$

where dX is depth of a pore per one segment ($dX = X/N$). An equation related to current flow in the electrolyte and at the electrode surface by Kirchhoff's voltage law was derived in order to express the impedance of pore electrode by TLM. There are the mesh current method and the branch current method for the calculation method by Kirchhoff's voltage law. The mesh current method was employed in this analysis because it is easy to express the equations by a matrix. Fig. 3 shows the relation between TLM and the current loops, I_1 is total current, I_k ($k = 2$–n) is current of loop k. The equations of the potential drops for the current loops in TLM equivalent circuit are summarized

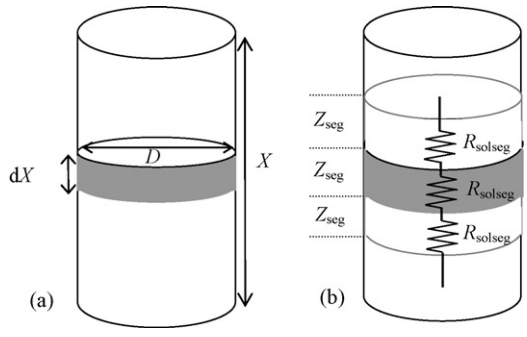

Fig. 4. (a and b) Conceptual model for single pore electrode.

as follows:

$$\left.\begin{aligned} E &= \left\{\sum_{n=1}^{N-1} R_{\text{solseg}} + Z_{\text{seg}}\right\} I_1 + \sum_{n=2}^{N-1} R_{\text{solseg}} I_n \\ &\quad + (R_{\text{solseg}} + Z_{\text{seg}}) I_N \\ 0 &= R_{\text{solseg}} I_1 + \left\{R_{\text{solseg}} + 2Z_{\text{seg}}\right\} I_2 - Z_{\text{seg}} I_3 \\ 0 &= R_{\text{solseg}} I_1 - Z_{\text{seg}} I_{n-1} + \left\{R_{\text{solseg}} + 2Z_{\text{seg}}\right\} I_n \\ &\quad - Z_{\text{seg}} I_{n+1} \\ &(n = 2, 3, \ldots, N-1) \\ 0 &= \left\{R_{\text{solseg}} + 2Z_{\text{seg}}\right\} I_1 - Z_{\text{seg}} I_{N-1} \\ &\quad + \left\{R_{\text{solseg}} + 2Z_{\text{seg}}\right\} I_N \end{aligned}\right\} \quad (9)$$

where E is the potential modulation of the electrode. These equations are expressed by a matrix M as follows:

$$\begin{pmatrix} E \\ 0 \\ 0 \\ \vdots \\ 0 \\ 0 \end{pmatrix} = M \begin{pmatrix} I_1 \\ I_2 \\ I_3 \\ \vdots \\ I_{N-1} \\ I_N \end{pmatrix} \quad (10)$$

where,

$$M = \begin{pmatrix} \sum_{N=1}^{N-1} R_{\text{solseg}} + Z_{\text{seg}} & R_{\text{solseg}} & R_{\text{solseg}} & \cdots & R_{\text{solseg}} & R_{\text{solseg}} + Z_{\text{sol}} \\ R_{\text{solseg}} & R_{\text{solseg}} + 2Z_{\text{sol}} & -Z_{\text{sol}} & 0 & \cdots & 0 \\ R_{\text{solseg}} & -Z_{\text{sol}} & \ddots & \ddots & & \vdots \\ \vdots & 0 & \ddots & \ddots & \ddots & 0 \\ R_{\text{solseg}} & \vdots & & \ddots & \ddots & -Z_{\text{sol}} \\ R_{\text{solseg}} + Z_{\text{sol}} & 0 & \cdots & 0 & -Z_{\text{sol}} & R_{\text{solseg}} + 2Z_{\text{sol}} \end{pmatrix} \quad (11)$$

The currents I_1–I_N can be assessed by using inverse matrix M^{-1} of Eq. (11).

$$\begin{pmatrix} I_1 \\ I_2 \\ I_3 \\ \vdots \\ I_{N-1} \\ I_N \end{pmatrix} = M^{-1} \begin{pmatrix} E \\ 0 \\ 0 \\ \vdots \\ 0 \\ 0 \end{pmatrix} \quad (12)$$

Impedance Z can be calculated from Eq. (13).

$$Z = \frac{E}{I_1} \quad (13)$$

In order to confirm the suitability of the algorithm and the calculation method of the present simulation, the impedance calculated by Eqs. (12) and (13) is shown in Fig. 5 with the results calculated by theoretical expression (1). Both plots are perfectly identical, indicating that impedance of distributed constant-typed equivalent circuit can be calculated by using the matrix. In this calculation, the segment number N was 200. The software for the matrix calculation was Matlab. Though the values of R^*_{sol}, R^{**}_{c}, and C^{**}_{dl} were constant to calculate the impedance in Fig. 5, the impedance of pore electrode which has other shape except for cylinder can be calculated by the same algorithm.

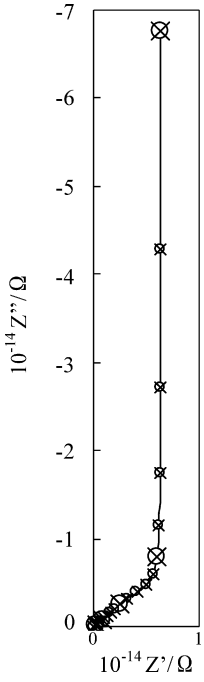

Fig. 5. Calculated result of electrochemical impedance of single pore electrode. (◯) Calculation with the present method using matrix, (×) calculation according to Eq. (1); (*X*) 75 nm, (*D*) 50 nm, (C^{**}_{dl}) 2.0×10^{-4} F/cm^2, and (ρ) 5.0×10^8 Wcm.

2.4. Impedance simulation of pore electrode with repeated structure

The electrode model with repeated structure is proposed to express the fractal structure of porous carbon electrode. A single pore of activated carbon is simulated by the cylindrical pore, and the fractal structure of activated carbon illustrated in Fig. 1 is expressed by the electrode model with repeated structure as depicted in Fig. 6(a). The secondary pore is located at bottom of the primary pore, and the third pore is located at the bottom

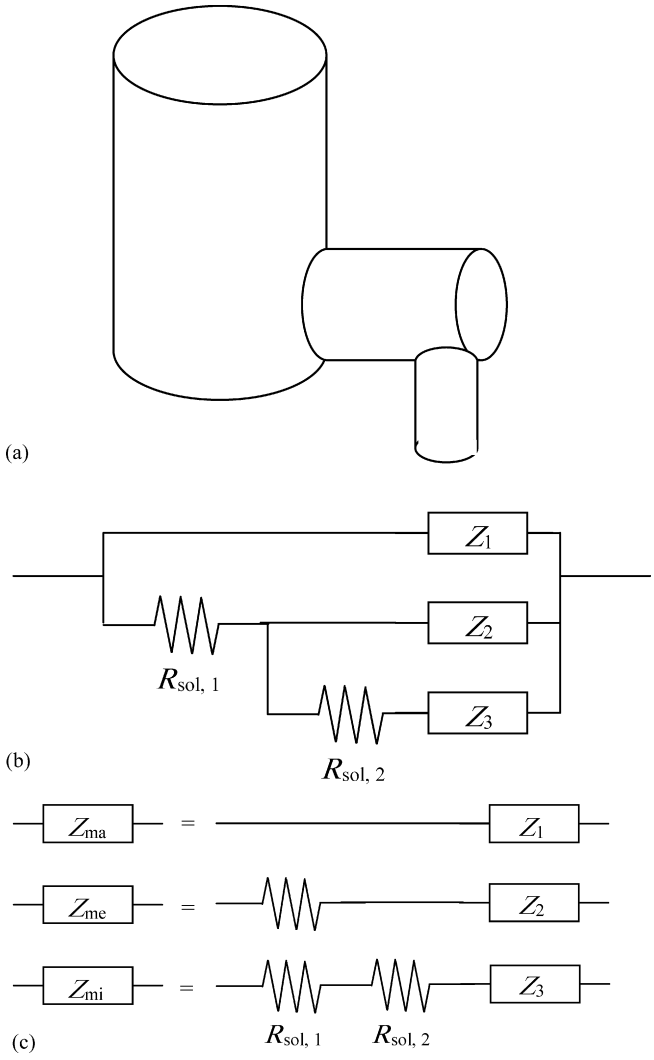

Fig. 6. (a) Conceptual model for pore electrode with repeated structure, (b) equivalent circuit for pore electrode with repeated structure, and (c) simplified equivalent circuit of pore electrode with repeated structure.

of the secondary pore subsequently. The equivalent circuit for the repeated pore structure is shown in Fig. 6(b), where Z_m is the impedance of mth pore. The solution resistance $R_{sol,m}$ of mth pore is expressed by Eq. (14),

$$R_{sol,m} = \sum_{n=1}^{N} R_{solseg,m} \tag{14}$$

where $R_{solseg,m}$ means solution resistance per one segment of mth pore. The total impedance of pore electrode with repeated structure Z_{total} is expressed by Eq. (15).

$$\frac{1}{Z_{total}} = \frac{1}{Z_1} + \frac{1}{R_{sol,1} + 1/((1/Z_2) + (1/(R_{sol,2} + Z_3)))} \tag{15}$$

The equivalent circuits of three kinds of pores are shown in Fig. 6(c). The impedance of macro pore Z_{ma} is identical to that of primary pore Z_1.

$$Z_{ma} = Z_1 \tag{16}$$

The impedance of meso pore Z_{me} is series of $R_{sol,1}$ and Z_2.

$$Z_{me} = Z_2 + R_{sol,1} \tag{17}$$

In addition the impedance of micro pore Z_{mi} is series of $R_{sol,1}$, $R_{sol,2}$, and Z_3.

$$Z_{mi} = Z_3 + R_{sol,1} + R_{sol,2} \tag{18}$$

Branch number of meso pore against macro pore is defined as b_1 and that of micro pore against meso pore is defined as b_2. In case that b_1 or b_2 is larger than unity, Z_{total} is expressed by Eq. (19).

$$\frac{1}{Z_{total}} = \frac{1}{Z_1} + \frac{1}{R_{sol,1} + 1/(b_1((1/Z_2) + (1/(R_{sol,2} + b_2 Z_3))))} \tag{19}$$

And

$$Z_{ma} = Z_1 \tag{20}$$

$$Z_{me} = R_{sol,1} + \frac{Z_2}{b_1} \tag{21}$$

$$Z_{mi} = R_{sol,1} + \frac{R_{sol,2} + (Z_3/b_2)}{b_1} \tag{22}$$

For example, the scheme of electrode model of brunch pore structure with $b = 3$ and the equivalent circuit are shown in Fig. 7(a and b). This model has the structure in which three meso pores exist at the bottom of one macro pore and three micro pores also exist at the bottom of one meso pore. The equivalent circuits of three kinds of pores are shown in Fig. 7(c). The impedance of macro pore Z_{ma} is the same as Z_1. The impedance of meso pore Z_{me} is composed of $R_{sol,1}$ and three Z_2. Furthermore, the impedance of micro pore Z_{mi} is composed of $R_{sol,1}$, three $R_{sol,2}$, and nine Z_3.

3. Experimental method

3.1. Electrochemical impedance measurement

EDLC by HONDA R&D (Ultra capacitor) shown in Fig. 8 was used for electrochemical impedance measurement. Potentiostat (Hokuto, HG-501G) and frequency response analyzer (Solartron, SI 1254) were equipped to measure the impedance spectra. The frequency range of impedance was from 10 mHz to 1 kHz, and the frequency of imposed signal was scanned logarithmically at 5 point for each decade from the high frequency region. The measurements were carried out by galvanostat mode and the amplitude of the sinusoidal input current was controlled to make the amplitude of ac potential response smaller than 10 mV.

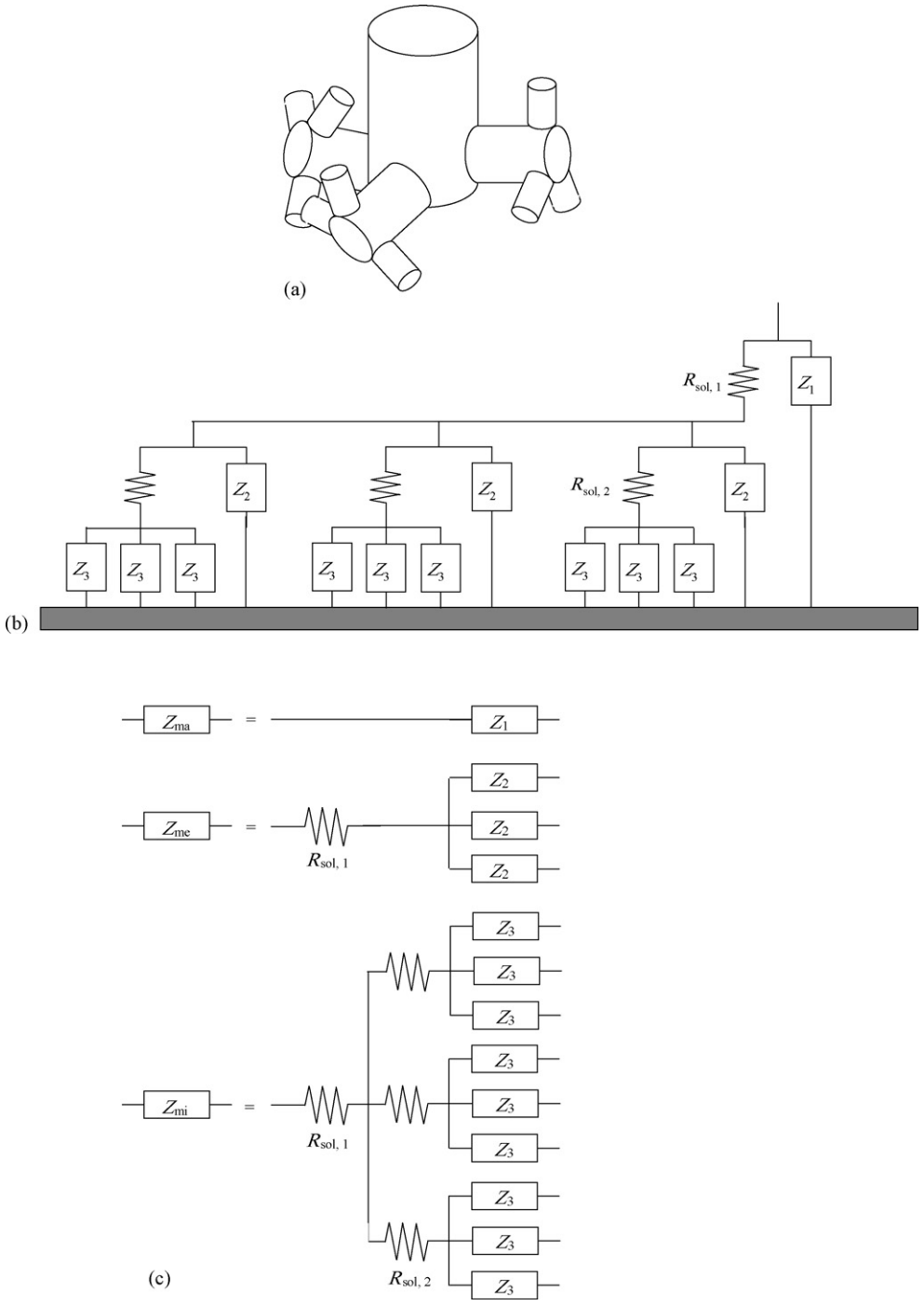

Fig. 7. (a–c) Conceptual model of pore electrode with branch structure.

4. Results and discussion

4.1. Electrochemical impedance measurement of EDLC

Experimental result of electrochemical impedance of EDLC at the bias voltage of 2.0 V is shown in Fig. 9. Impedance spectrum can be divided into two frequency ranges, namely, the distributed constant range above 100 mHz and the lumped constant range below 100 mHz. The real part of impedance is constant, and the imaginary part increases with the decrease of the frequency at lumped constant range, indicating the blocking electrode behavior in the low frequency range. Impedance deviates from the locus of blocking electrode at distributed constant range. It is considered that the current distribution is non-uniform by porous structure of electrode in the high frequency range. The solution resistance at high frequency limit is approximately 0.002 Ω, indicating the low contact resistance and electrolyte resistance of the present EDLC.

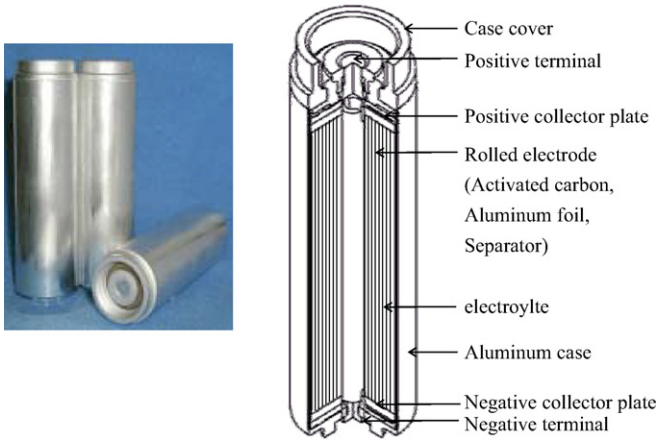

Fig. 8. Photograph of scheme of EDLC manufactured by Honda R&D.

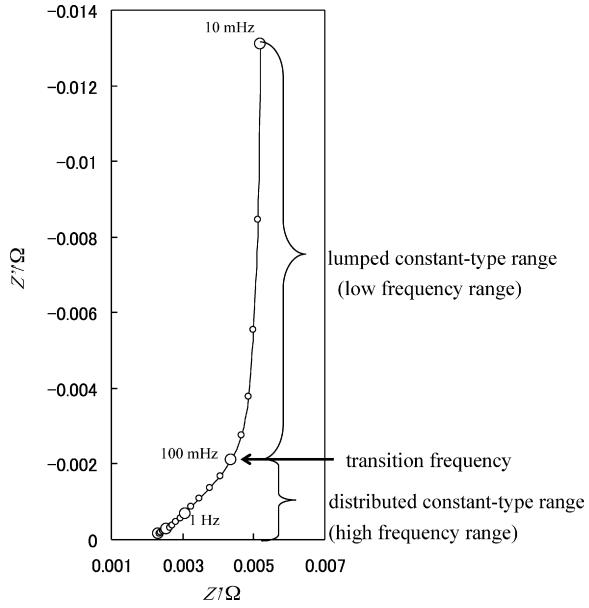

Fig. 9. Experimental result of electrochemical impedance of EDLC, frequency range: 1 kHz–10 mHz, charging voltage: 2.0 V, and measurement temperature: 278 K.

4.2. Computer simulation of electrochemical impedance with TLM

4.2.1. Influences of various parameters on the simulated results of electrochemical impedance

The results of electrochemical impedance calculated by Eq. (15) are shown in Fig. 10. All impedance spectra described the locus of lumped and distributed constant-types in low and high frequency ranges, respectively. Fig. 10(a) shows the simulated results of electrochemical impedance with variations of depths of macro, meso, and micro pores. Depths of macro, meso, and micro pores are defined as X_{ma}, X_{me}, and X_{mi}, respectively. The transition frequency shifts to low frequency side with the increases of X_{ma}, X_{me}, and X_{mi}. This result indicates that the

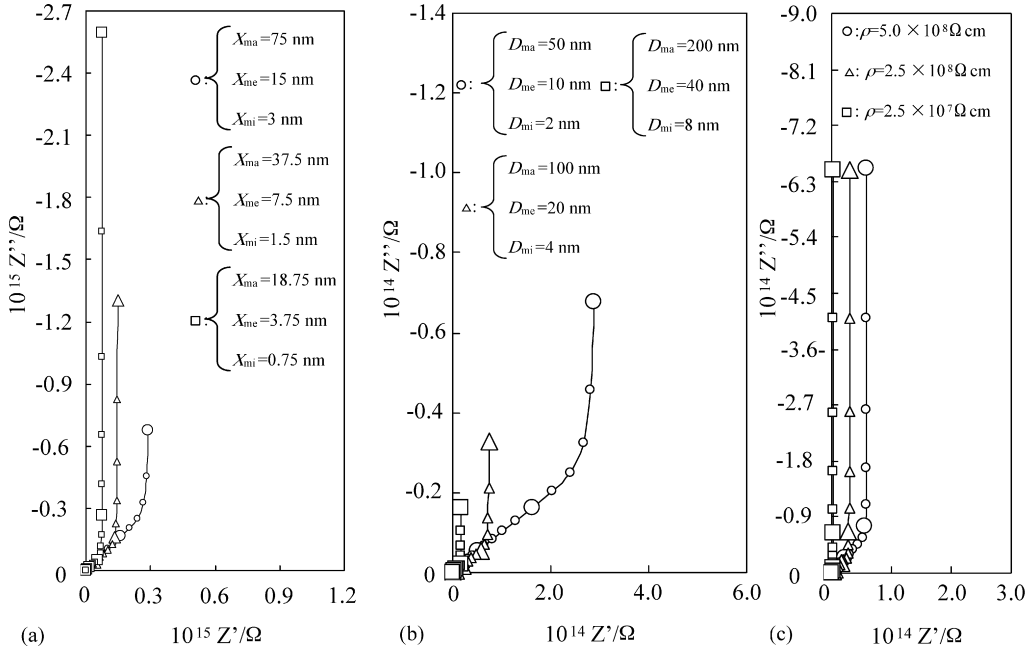

Fig. 10. Dependence of various parameters on the simulated results of electrochemical impedance of pore electrode with repeated structure (a) dependence of pore depth. The values of pore depth are indicated in Fig. 9(a). D_{ma}: 50 nm, D_{me}: 10 nm, D_{mi}: 2 nm, C_{dl}^{**} : 2.0×10^{-4} F/cm^2, ρ: 5.0×10^8 Ω cm, (◯) X_{ma}: 75 nm, X_{me}: 15 nm, X_{mi}: 3 nm, (△) X_{ma}: 37.5 nm, X_{me}: 7.5 nm, X_{mi}: 1.5 nm, (□) X_{ma}: 18.75 nm, X_{me}: 3.75 nm, X_{mi}: 0.75 nm and (b) dependence of diameter of a pore. The values of pore depth are indicated in (b), X_{ma}: 75 nm, X_{me}: 15 nm, X_{mi}: 3 nm, C_{dl}^{**} : 2.0×10^{-4} F/cm^2, ρ: 5.0×10^8 Ω cm, (◯) D_{ma}: 50 nm, D_{me}: 10 nm, D_{mi}: 2 nm, (△) D_{ma}: 100 nm, D_{me}: 20 nm, D_{mi}: 4 nm, (□) D_{ma}: 200 nm, D_{me}: 40 nm, D_{mi}: 8 nm and (c) dependence of specific resistance. The values of pore depth are indicated in (c), X_{ma}: 75 nm, D_{ma}: 50 nm, X_{me}: 15 nm, D_{me}: 10 nm, X_{mi}: 3 nm, D_{mi}: 2 nm, C_{dl}^{**} : 2.0×10^{-4} F/cm^2, (◯) 5.0×10^8 Ω cm, (△) 2.5×10^8 Ω cm, (□) 2.5×10^7 Ω cm.

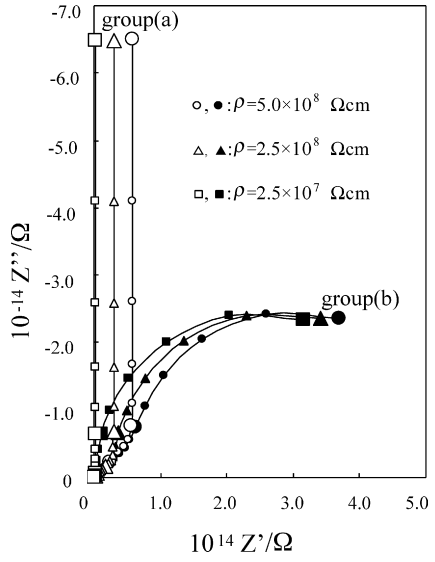

Fig. 11. Dependence of the equivalent circuit of electrode/solution interface on the simulated results of electrochemical impedance of pore electrode with repeated structure changed. (a) The case that equivalent circuit includes Faradic process and consists of R^{**} and C_{dl}^{**}. The value of ρ is written in Fig. 10(a), X_{ma}: 75 nm, D_{ma}: 50 nm, X_{me}: 15 nm, D_{me}: 10 nm, X_{mi}: 3 nm, D_{mi}: 2 nm, C_{dl}^{**}: 2.0×10^{-4} F/cm^2, ●: 5.0×10^8 Ω cm, ▲: 2.5×10^8 Ω cm, and ■: 2.5×10^7 Ω cm. (b) The case that equivalent circuit exclude faradic process, X_{ma}: 75 nm, D_{ma}: 50 nm, X_{me}: 15 nm, D_{me}: 10 nm, X_{mi}: 3 nm, D_{mi}: 2 nm, R_c^{**}: 6.0×10^4 Ω cm, C_{dl}^{**}: 2.0×10^{-4} F/cm^2, ◯: 5.0×10^8 Ω cm, △: 2.5×10^8 Ω cm, and □: 2.5×10^7 Ω cm.

current distribution becomes non-uniform since the solution resistance between top and bottom of pores increases with the increase of X. In addition, the absolute value of impedance in lumped constant-type range decreases with the increase of X because surface area of inner wall of pores increases. Fig. 10(b) shows the simulated results of electrochemical impedance with the variations of diameter of macro, meso, and micro pores. Diameter of macro, meso, and micro pores are defined as D_{ma}, D_{me}, and D_{mi}, respectively. The transition frequency shifts to low frequency side with the decrease of D because the solution resistance in the pores increases with the decrease of the cross-section area. Furthermore, the absolute value of impedance in the lumped constant-type range increases since the area of the electrode/electrolyte interface decreases with the decrease of D. Fig. 10(c) shows simulated results of electrochemical impedance with the variations of specific resistance ρ. The transition frequency shifts to low frequency side with the increase of ρ because the solution resistance in the pores increases. The value of imaginary part does not change depending on the ρ because the solution resistance influences on the high frequency impedance. Fig. 11 shows simulated results of electrochemical impedance of different interfacial impedance at electrolyte/electrode interface. Open symbols (group (a)) denote the impedance when the interfacial impedance is compose of the only capacitance C_{dl}^{**}, and solid symbols (group (b)) denote the impedance when the interfacial impedance has the time constant of reaction resistance R_c^{**} and capacitance C_{dl}^{**}. The impedance spectra of the groups (a) and (b) agree in the distributed constant-type range. Contrary to this, the impedance spectra of groups (a) and (b) in lumped constant-type range describe vertical straight line and semicircle, respectively. These results mean that the interfacial impedance of electrode/electrolyte interface Z^{**} controlled the shape of impedance spectrum in the lumped constant-type range. It was found from the simulated results in Figs. 10 and 11 that the interfacial impedance and pore dimension control the impedance in the lumped constant-type range and that the ρ and pore dimension control the impedance in the distributed constant-type range.

Simulated results of electrochemical impedance with various number of b are shown in Fig. 12. In the case (a) that $b_1 = 4$, $b_2 = 16$, the impedance describes the locus of lumped and distributed constant-types in low and high frequency ranges, respectively and almost agree with that in Fig. 5. However, the real axis and transition frequency is unclear. In the case (b) that $b_1 = 10$, $b_2 = 100$, the transition frequency cannot be distinguished and the angle of straight line in the high frequency range is smaller than 45°. In the case (c) that $b_1 = 100$, $b_2 = 10{,}000$, the locus of semicircle appears in distributed constant range. The reason is that the time constant of impedance of micro pore Z_{mi} is small value since the solution resistance from electrode surface to the micro pore ($R_{sol,1} + R_{sol,2}$) is small.

4.2.2. Curve-fitting of electrochemical impedance of EDLC

On the basis of the simulated results in Section 4.2.1, the curve-fitting to electrochemical impedance of EDLC was carried out. The fitted result is shown in Fig. 13 with the experimental results. The fitting parameters are as follows: $X_{ma} = 75$ nm, $D_{ma} = 50$ nm for macro pore, $X_{me} = 15$ nm, $D_{me} = 10$ nm for meso pore, $X_{mi} = 3$ nm, $D_{mi} = 2$ nm for micro pore, $C_{dl}^{**} = 3.0 \times 10^{-5}$ F/cm^2, $\rho = 2.5 \times 10^9$ Ω cm, $b_1 = 2$, $b_2 = 10$, and number of pores is 2.0×10^{17}. The resistance of solution bulk R_{bulk} was assumed as 2.2×10^{-3} Ω, and was added to the calculated impedance. The simulated result of electrochemical impedance with this method is in good agreement with the experimental one in Fig. 13. The diameter of a pore D is generally that macro pore over 50 nm, meso pore 50–2 nm, and micro pore under 2 nm. Song et al. [20] carried out the curve-fitting to impedance spectrum of EDLC with mode radius 0.33 μm of pore distribution by TLM-PSD. Since the pore size of activated carbon has wide distribution with a few modes models of nm order [6,7], the electrode pore structure of EDLC was expressed by three kinds of pores of nm orders in the present analysis. The capacitance per unit area C_{dl}^{**} was 3.0×10^{-5} F cm^{-2} in this simulation, and this value was similar to reported ones 3.0×10^{-5} F cm^{-2} by Srinivasan et al. [11], 3.0×10^{-5} F cm^{-2} by Candy et al. [10] and 2.5×10^{-5} F cm^{-2} by Song et al. [20]. It was assumed that the specific resistance of electrolyte was 66.7 Ω cm in this simulation. This value is quite huge comparing with the specific resistance of general organic electrolyte because the ion migration is restricted in the pore whose size is 1–10 nm and the electric double layer also influences on the ion migration in particular. In this simulation, the specific capacitance ρ in all pores was constant value, and more accurate

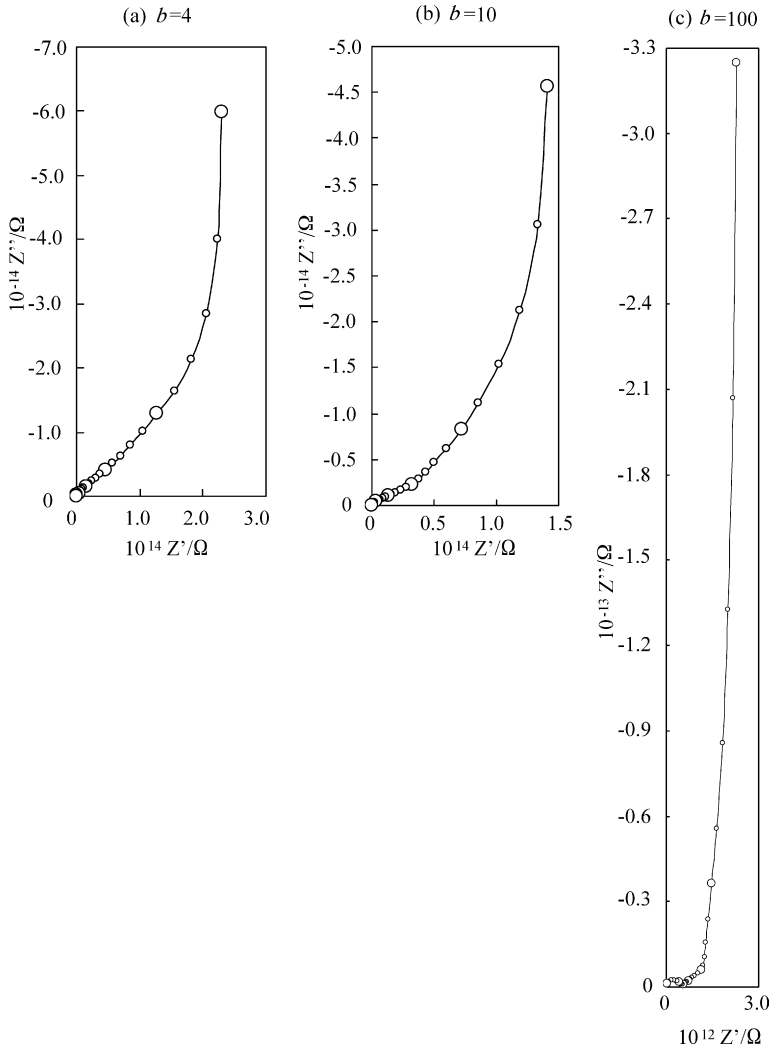

Fig. 12. Simulated results of electrochemical impedance of pore electrode with branch structure. The numbers of branch b are (a) 4, (b) 10 and (c) 100. X_{ma}: 75 nm, D_{ma}: 50 nm, X_{me}: 15 nm, D_{me}: 10 nm, X_{mi}: 3 nm, D_{mi}: 2 nm, C_{dl}^{**} : 2.0×10^{-4} F/cm^2, ρ: 5.0×10^8 Ω cm, frequency range: (a–c) 10 mHz–10 kHz.

analysis can be carried out to assume the different ρ for each pore.

The merit of the present analysis is that the impedance spectra for macro, meso, micro pores can be separated in course of the curve-fitting to impedance spectrum. Furthermore, resistance R_M and capacitance C_M for each pore are determined by following formulas:

$$Z_M = Z'_M - jZ''_M \quad (23)$$

$$R_M = Z'_M \quad (24)$$

$$C_M = \frac{1}{\omega Z''_M} \quad (25)$$

In Eqs. (20)–(22), the subscript M represents the kind of pore; M = ma, me, and mi means macro, meso, and micro pores, respectively. The R_M, C_M calculated by Eqs. (20)–(22) are shown in Fig. 14. In Fig. 14(a), the resistance is constant value at low and high frequency range, and decreases with the increase of frequency in the transition frequency range from 0.1 to 1 Hz. This transition frequency in Fig. 14(a) almost agreed with that in Fig. 13. The order of resistance was $R_{mi} > R_{me} > R_{ma}$ in high frequency range because R_{ma} corresponds to the bulk solution resistance R_{bulk} and R_{me} and R_{mi} includes the solution resistance in the pores in high frequency range. Resistance in low frequency range is larger than that in high frequency range in Fig. 14(a). For example, R_{ma} involves not only R_{bulk} but also the solution resistance in macro pore in low frequency range because the current flows to all inner wall of macro pore for charge and discharge. The frequency-dependent capacitance for each pore is shown in Fig. 14(b). The capacitance has maximum value in low frequency range, and decreases with the increase of the frequency. The order of capacitance is $C_{ma} > C_{me} > C_{mi}$ in low frequency range. The ratio of low frequency capacitance of macro, meso, and micro pores is 27.05:2.49:1, and the ratio of surface area is 31.25:2.50:1, which is calculated from fitting parameters for each pore. Therefore, it can be considered that the low frequency capacitance is in proportion to the surface area with regardless the kind of pore.

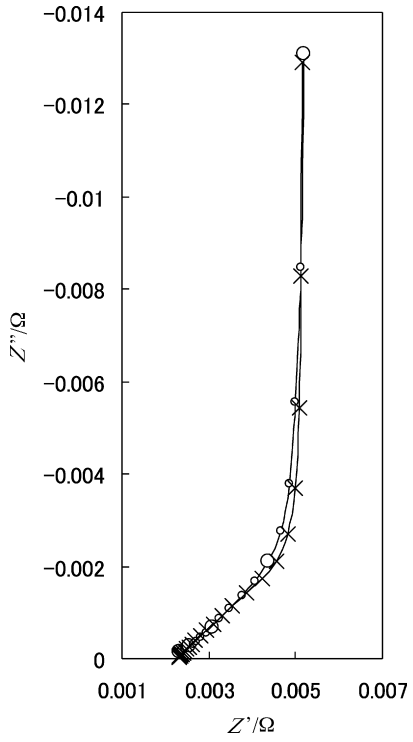

Fig. 13. Experimental and fitted results of electrochemical impedance of EDLC. The parameters for curve fitting are as follows. X_{ma}: 75 nm, D_{ma}: 50 nm, X_{me}: 15 nm, D_{me}. 10 nm, X_{mi}: 3 nm, D_{mi}: 2 nm, C_{dl}^{**} : 3.0×10^{-5} F/cm^2, ρ: 2.5×10^8 Ω cm, b_{me}: 10, b_{mi}: 50, and number of pore: 2.0×10^{17}.

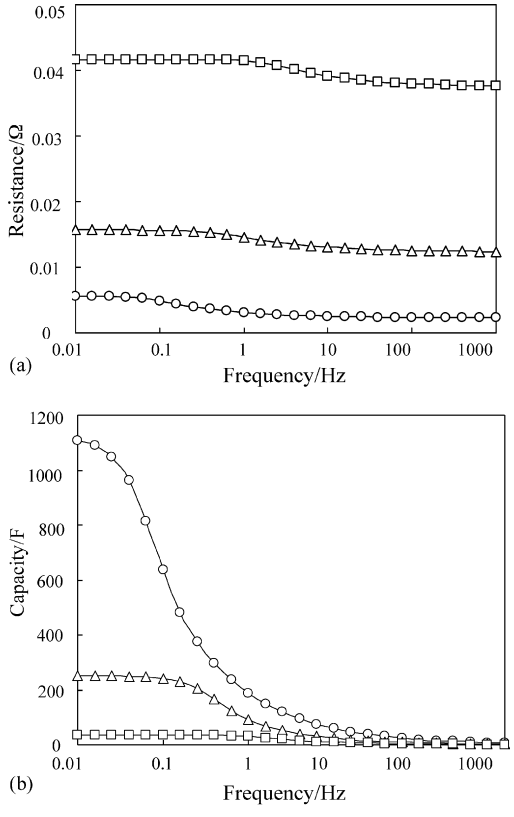

Fig. 14. The result of resistance, capacitance, and time constant calculated from Z_{ma}, Z_{me}, and Z_{mi}. (a) The results of relationship resistance and frequency: (◯) R_{ma}, (△) R_{me}, and (□) R_{mi}; (b) the results of relationship capacitance and frequency: (◯) C_{ma}, (△) C_{me}, and (□) C_{mi}.

5. Conclusions

A new electrode model with TLM was proposed for EDLC. The impedance of EDLC described locus of blocking electrode in low frequency range and the curve at an angle of almost 45° to real axis in high frequency range on the Nyquist plane since current distribution becomes non-uniform in high frequency range by porous structure of electrode surface. Computer simulation of electrochemical impedance with the present electrode model was carried out. The contribution of five parameters to impedance spectrum was discussed, i.e., depth of pore, diameter of pore, specific resistance, the equivalent circuit of electrode/solution interface, and branch number. The branch number b influenced on the shape of impedance spectrum in distributed constant-type range significantly. On other hand, the interfacial impedance at electrode/solution interface controlled the shape of the impedance spectrum in lumped constant-type range. Depth of pore X, diameter of pore D, and specific capacitance ρ influence the transition frequency. In addition, X and D influence absolute value of impedance in lumped constant-type range. On the other hand, ρ does not influence absolute value of impedance in lumped constant-type range. The resistance and capacitance for each pore was determined as a function of frequency, and the efficiency of charge and discharge in each pore was discussed.

References

[1] G. Salitra, A. Soffer, L. Eliad, Y. Cohen, D. Aurbach, J. Electrochem. Soc. 147 (2000) 2486.
[2] S. Shiraishi, H. Kurihara, A. Oya, Electrochemistry 69 (2001) 440.
[3] S. Shiraishi, H. Kurihara, A. Oya, Carbon 41 (2003) 1765.
[4] Y. Matsuda, Tanso 216 (2005) 41.
[5] G. Gryglewicz, J. Machinikowshi, E.L. Grabowska, G. Lota, E. Frackwiak, Electrochim. Acta 50 (2005) 1197.
[6] D. Qu, H. Shi, J. Power Sources 74 (1998) 99.
[7] C. Lin, J.A. Ritter, B.N. Popov, J. Electrochem. Soc. 146 (1999) 3639.
[8] M. Endo, T. Maeda, T. Takeda, Y.J. Kim, K. Koshiba, H. Hara, M.S. Dresselhaus, J. Electrochem. Soc. 148 (2001) A910.
[9] H. Keiser, K.D. Beccu, M.A. Gutjahr, Electrochim. Acta 21 (1976) 539.
[10] J.P. Candy, P. Fouilloux, Electrochim. Acta 26 (1981) 1029.
[11] V. Srinivasan, J.W. Weidner, J. Electrochem. Soc. 146 (1999) 1650.
[12] K. Honda, T.N. Rao, D.A. Tryk, A. Fujishima, M. Watanabe, K. Yasui, H. Masuda, J. Electrochem. Soc. 148 (2001) A668.
[13] P.L. Taberna, P. Simon, J.F. Fauvarque, J. Electrochem. Soc. 150 (2003) A292.
[14] F. Lufrano, P. Stati, M. Minutoli, J. Power Sources 124 (2003) 314.
[15] E. Lust, A. Jaenes, M. Arulepp, J. Electrochem. Soc. 562 (2004) 33.
[16] J.H. Jang, S.M. Oh, J. Electrochem. Soc. 151 (2004) A571.
[17] S. Yooh, J.H. Jang, B.H. Ka, S.M. Oh, Electrochim. Acta 50 (2005) 2255.
[18] J.H. Jang, S. Yooh, B.H. Ka, S.M. Oh, J. Electrochem. Soc. 152 (2005) A1418.
[19] H.K. Song, Y.H. Jung, K.H. Lee, Electrochim. Acta 44 (1999) 3513.
[20] H.K. Song, H.Y. Hwang, K.H. Lee, L.H. Dao, Electrochim. Acta 45 (2000) 2241.
[21] R.D. Levie, Electrochim. Acta 8 (1963) 751.
[22] M. Itagaki, M. Igarashi, K. Watanabe, Electrochemistry 70 (2002) 686.